2018 European Control Conference (ECC)
June 12-15, 2018. Limassol, Cyprus

Convergence of Dynamical Movement Primitives with Temporal Coupling

Martin Karlsson* Anders Robertsson Rolf Johansson

***Abstract*— In this paper, it is shown that temporally coupled dynamical movement primitives (DMPs), used to model and execute robot movements, are globally exponentially stable. It follows that DMPs converge to their goal configurations, which is necessary to accomplish most tasks. The convergence is proven mathematically, and then verified in simulations as well as experimentally on an industrial robot.**

I. Introduction

Industrial robots commonly operate by executing sequences of predefined motion trajectories, with high position accuracy, but with little or no ability to adjust for unforeseen changes in the surroundings. Therefore, very carefully prepared work-spaces and robot programs are required, which implies high costs for engineering work, and prohibits the automatization of a wide range of tasks, such as assembly tasks and short-series production.

To enhance replanning capabilities of robots, the framework of dynamical movement primitives (DMPs) for motion modeling has been developed. Early versions were introduced in [1], [2], [3], and a review can be found in [4]. Online motion modulation using DMPs has been widely considered in the literature. For instance, adaptation based on force/torque measurements was developed in [5], obstacle avoidance was explored in [4], [6], and DMPs with compliant behavior were developed in [7], [8]. Functionality for modification of DMPs by means of lead-through programming was presented in [9], [10].

It was demonstrated in, *e.g.*, [4], that robot movements generated by original DMPs do not perform satisfactorily after the robot has been subject to perturbations. One reason for this is that in the original DMP formulation the evolution of the phase variable is unaffected by any perturbation, which commonly results in significant deviation from the intended trajectory even after the cause of the perturbation has vanished. In [4], it was also suggested to solve this problem by augmenting the DMP framework to include temporal coupling. Though promising, the suggested augmentation was not practically realizable until it was modified in [11].

* The authors work at the Department of Automatic Control, Lund University, PO Box 118, SE-221 00 Lund, Sweden.
HK May 15 2013 Martin.Karlsson@control.lth.se
The authors would like to thank Jacek Malec, Mathias Haage and Elin Anna Topp at Computer Science, Lund University, as well as Fredrik Bagge Carlson and Björn Olofsson at Dept. Automatic Control, Lund University, for valuable discussions throughout this work. The authors are members of the LCCC Linnaeus Center and the ELLIIT Excellence Center at Lund University. The research leading to these results has received funding from the Vinnova project *Kirurgens Perspektiv* and the European Commission's Framework Programme Horizon 2020 – under grant agreement No 644938 – SARAFun.

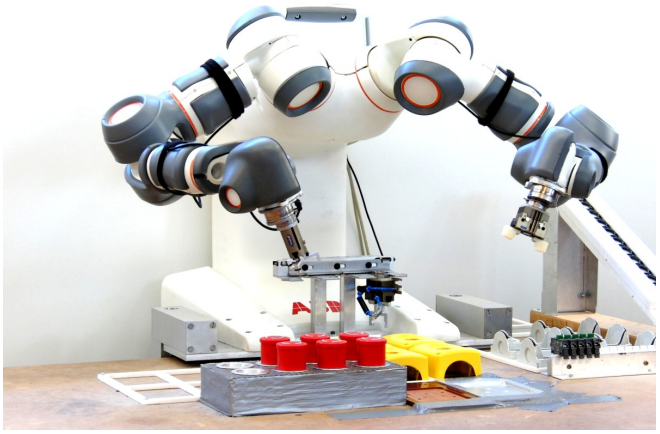

Fig. 1: The ABB YuMi [14] prototype robot used in the experiments.

More details on why temporal coupling is necessary in the presence of possible perturbations can be found in [4], [11].

Stability for the original DMP framework, *i.e.*, not including temporal coupling, was concluded in [12], [13]. The aim of this paper is to provide a stability analysis for temporally coupled DMPs, as formulated in [11]. This is addressed in three ways; first by a mathematical analysis, thereafter by simulations, and finally experimentally using an industrial robot, shown in Fig. 1.

To facilitate the understanding of the research presented, a video is available in [15]. In Part I of the video, the experimental setups are shown, except that the temporally coupled DMPs were executed without any perturbations present. This is to visualize what should be achieved by the robot, in each setup. In Part II, DMPs without temporal coupling were used, and the robot was subject to perturbations. The purpose of this part is to demonstrate that the robot risks to fail in such a scenario, and hence motivate why temporal coupling is necessary. This risk of failure was also indicated in [4], using one-dimensional simulation examples. Part III of the video shows the experiments presented in Secs. V and VI, where temporally coupled DMPs were executed in the presence of perturbations.

A. Problem formulation

DMPs with temporal coupling have shown promising properties in practice [11], but to the best of our knowledge, it has hitherto not been shown whether these are stable, and whether convergence to the goal configuration could be guaranteed. Unstable robot motion control could damage the

TABLE I: Notation used in this paper.

Notation	Space	Description
n	$\in \mathbb{Z}^+$	Dimension of robot position
y_a	$\in \mathbb{R}^n$	Actual robot position
g	$\in \mathbb{R}^n$	Goal position
y_c	$\in \mathbb{R}^n$	Coupled robot position
$\alpha_z, \beta_z, k_v, k_p$	$\in \mathbb{R}^+$	Constant control coefficients
τ	$\in \mathbb{R}^+$	DMP time constant
τ_a	$\in \mathbb{R}^+$	Adaptive time parameter
x	$\in \mathbb{R}^+$	Phase variable
α_x, α_e, k_c	$\in \mathbb{R}^+$	Positive constants
y_0	$\in \mathbb{R}^n$	Initial robot position
$f(x)$	$\in \mathbb{R}^n$	Learnable virtual forcing term
N_b	$\in \mathbb{Z}^+$	Number of basis functions
$\Psi_j(x)$	$\in \mathbb{R}^n$	The j:th basis function vector
w_j	$\in \mathbb{R}^n$	The j:th weight vector
e	$\in \mathbb{R}^n$	Low-pass filtered $y_a - y_c$
$\ddot{y}_r$	$\in \mathbb{R}^n$	Reference robot acceleration
ξ	$\in \mathbb{R}^{5n+1}$	State vector

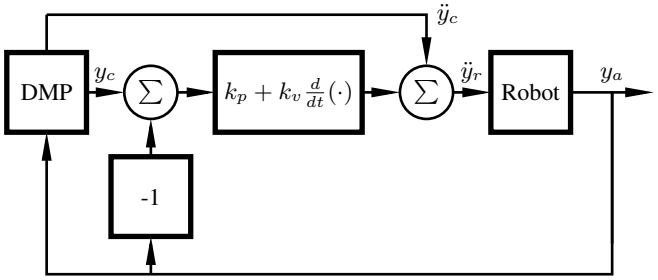

Fig. 2: The control structure for temporally coupled DMPs. The block denoted 'Robot' includes the internal controller of the robot. The 'DMP' block corresponds to the computations in (1) – (7), and the PD controller together with the feedforward term $\ddot{y}_c$ is specified in (8).

robot and its surroundings, such as tooling and workpieces. Further, in robotic manipulation, it is crucial that the robot reaches its goal configuration in each of its movements. If this would not be achieved, sub-tasks would likely be left incomplete, yielding unforeseen hardware configurations, which in turn could result in collision and broken hardware. For temporally coupled DMPs to be used in a larger scale in the future, it is therefore necessary to prove that these result in stable behavior.

In this paper, we therefore address the question of whether temporally coupled DMPs, presented in [11], are stable, and whether they converge to their respective goal configuration. More specifically, we investigate whether the closed-loop control system in (11) is globally exponentially stable. A mathematical definition of exponential stability can be found in, *e.g.*, [16]. In words, a system is globally exponentially stable if the state vector converges to the origin faster than an exponentially decaying function.

II. Control Algorithm

The control algorithm for temporally coupled DMPs is detailed in [11], and for convenience it is briefly described in this section. Table I lists some of the notation used in this paper. A coupled DMP trajectory, y_c, is modeled by the dynamical system

$$\tau_a \dot{z} = \alpha_z(\beta_z(g - y_c) - z) + f(x) \tag{1}$$

$$\tau_a \dot{y}_c = z \tag{2}$$

Here, x is a phase variable that evolves as

$$\tau_a \dot{x} = -\alpha_x x \tag{3}$$

Further, $f(x)$ is a virtual forcing term, of which the parameters can be learned from a desired movement such as a demonstrated trajectory, and each element i of $f(x)$ is given by

$$f_i(x) = \frac{\sum_{j=1}^{N_b} \Psi_{i,j}(x) w_{i,j}}{\sum_{j=1}^{N_b} \Psi_{i,j}(x)} x \cdot (g_i - y_{0,i}), \tag{4}$$

where each basis function, $\Psi_{i,j}(x)$, is determined as

$$\Psi_{i,j}(x) = \exp\left(-\frac{1}{2\sigma_{i,j}^2}(x - c_{i,j})^2\right) \tag{5}$$

Here, σ and c denote the width and center of each basis function, respectively. Denote by y_a the actual configuration of the robot. The adaptive time parameter τ_a is determined based on the low-pass filtered difference between y_c and y_a as follows.

$$\dot{e} = \alpha_e(y_a - y_c - e) \tag{6}$$

$$\tau_a = \tau(1 + k_c e^T e) \tag{7}$$

Moreover, the controller below is used to drive y_a to y_c.

$$\ddot{y}_r = k_p(y_c - y_a) + k_v(\dot{y}_c - \dot{y}_a) + \ddot{y}_c \tag{8}$$

This is a PD controller, together with the feedforward of $\ddot{y}_c$. Here, $\ddot{y}_r$ denotes reference acceleration sent to the internal controller of the robot. We let $k_p = k_v^2/4$, so that (8) represents a critically damped control loop. The control system is schematically visualized in Fig. 2. We model the 'Robot' block as a double integrator, so that $\ddot{y}_a = \ddot{y}_r$, which is reasonable for accelerations of moderate magnitudes and changing rates. These properties were indicated in [11].

III. Mathematical Stability Analysis

In this section, we analyze the stability properties of temporally coupled DMPs. See also the Appendix, where passivity is shown. The entire control system described in Sec. II is given by

$$\begin{cases} \ddot{y}_a = k_p(y_c - y_a) + k_v(\dot{y}_c - \dot{y}_a) + \ddot{y}_c \\ \dot{e} = \alpha_e(y_a - y_c - e) \\ \tau_a = \tau(1 + k_c e^T e) \\ \tau_a \dot{x} = -\alpha_x x \\ \tau_a \dot{y}_c = z \\ \tau_a \dot{z} = \alpha_z(\beta_z(g - y_c) - z) + f(x) \end{cases} \tag{9}$$

We introduce the state vector ξ as

$$\xi = \begin{pmatrix} y_a - y_c \\ \dot{y}_a - \dot{y}_c \\ e \\ x \\ y_c - g \\ z \end{pmatrix} \tag{10}$$

assuming a contractible state space as discussed in Sec. VII, and write the system on state-space form,

$$\frac{d}{dt}\begin{pmatrix} y_a - y_c \\ \dot{y}_a - \dot{y}_c \\ e \\ x \\ y_c - g \\ z \end{pmatrix} = \begin{pmatrix} \dot{y}_a - \dot{y}_c \\ -k_p(y_a - y_c) - k_v(\dot{y}_a - \dot{y}_c) \\ \alpha_e(y_a - y_c - e) \\ -\frac{\alpha_x}{\tau_a}x \\ \frac{1}{\tau_a}z \\ \frac{\alpha_z}{\tau_a}(\beta_z(g - y_c) - z) + \frac{1}{\tau_a}f(x) \end{pmatrix} \tag{11}$$

The states $y_a - y_c$, $\dot{y}_a - \dot{y}_c$, and e have the same dimension, which we denote by n. Let I_n be the identity matrix, and 0_n the zero matrix, each of size n. The upper part of (11) is linear and can be written as

$$\frac{d}{dt}\begin{pmatrix} y_a - y_c \\ \dot{y}_a - \dot{y}_c \\ e \end{pmatrix} = \begin{pmatrix} 0_n & I_n & 0_n \\ -k_p I_n & -k_v I_n & 0_n \\ \alpha_e I_n & 0_n & -\alpha_e I_n \end{pmatrix}\begin{pmatrix} y_a - y_c \\ \dot{y}_a - \dot{y}_c \\ e \end{pmatrix} \tag{12}$$

Denote by ξ_1 and A_1 the state vector and the system matrix in (12), respectively.

Theorem 1: The dynamical system defined by (12) for DMP operation has $\xi_1 = 0$ as a globally exponentially stable equilibrium.

Proof: For $\xi_1 = 0$ we have $d\xi_1/dt = 0$ in (12), so $\xi_1 = 0$ is an equilibrium. The system is globally asymptotically stable if the real part of each eigenvalue of A_1 is strictly negative [17]. With $k_p = k_v^2/4$ (see Sec. II) the eigenvalues are given by

$$\begin{cases} \lambda_{1,\ldots,2n} = -\frac{k_v}{2} \\ \lambda_{2n+1,\ldots,3n} = -\alpha_e \end{cases} \tag{13}$$

These are strictly negative, since $k_v, \alpha_e > 0$. The linear system is hence globally asymptotically stable. For linear systems, asymptotic stability is equivalent with exponential stability [18], [16]. The system is therefore globally exponentially stable. ■

Next, we will show that the system given by

$$\frac{d}{dt}\begin{pmatrix} y_a - y_c \\ \dot{y}_a - \dot{y}_c \\ e \\ x \end{pmatrix} = \begin{pmatrix} \dot{y}_a - \dot{y}_c \\ -k_p(y_a - y_c) - k_v(\dot{y}_a - \dot{y}_c) \\ \alpha_e(y_a - y_c - e) \\ -\frac{\alpha_x}{\tau_a}x \end{pmatrix} \tag{14}$$

is contracting, of which a defition can be found in [19]. We note that this is a hierarchical system, consisting of (12), which does not depend on x, and of $\dot{x} = -\alpha_x x/\tau_a$. To show contraction, we will use the following proposition.

Proposition 1: If $\dot{x}_1 = g_1(x_1)$ is contracting, and $\dot{x}_2 = g_2(x_1, x_2)$ is contracting for each fixed x_1, then the hierarchy

$$\frac{d}{dt}\begin{pmatrix} x_1 \\ x_2 \end{pmatrix} = \begin{pmatrix} g_1(x_1) \\ g_2(x_1, x_2) \end{pmatrix} \tag{15}$$

is contracting. ■

This follows directly from Proposition 2 in [13], by applying it to autonomous systems.

Proposition 2: The system given by (14) is contracting.

Proof: We know from Theorem 1 that (12) is globally exponentially stable. It is therefore contracting [19]. For the fixed point $\xi_1 = 0$, we have $\dot{x} = -\alpha_x x/\tau$, which is contracting since $-\alpha_x/\tau < 0$. It now follows from Proposition 1 that the hierarchical combination (14) is contracting. ■

We now address the stability of the entire control system in (11) as follows.

Theorem 2: The system given by (11) for DMP operation has $\xi = 0$ as a globally exponentially stable equilibrium point.

Proof: Since x is a factor of $f(x)$ and the remaining part of $f(x)$ is bounded, $f(0) = 0$, see Sec. II and [4]. It can therefore be seen that $\xi = 0$ yields $d\xi/dt = 0$, so $\xi = 0$ is an equilibrium point. It remains to show the stability. We know from Proposition 2 that (14) is contracting, and it can be seen that it has the origin as a fixed point. Consider now the remaining part of (11), *i.e*,

$$\frac{d}{dt}\begin{pmatrix} y_c - g \\ z \end{pmatrix} = \begin{pmatrix} \frac{1}{\tau_a}z \\ \frac{\alpha_z}{\tau_a}(\beta_z(g - y_c) - z) + \frac{1}{\tau_a}f(x) \end{pmatrix} \tag{16}$$

For the fixed point of (14) we have $\tau_a = \tau$ and $f(x) = f(0) = 0$, and the system (16) then simplifies to

$$\frac{d}{dt}\begin{pmatrix} y_c - g \\ z \end{pmatrix} = \begin{pmatrix} 0_n & \frac{1}{\tau}I_n \\ -\frac{\alpha_z\beta_z}{\tau}I_n & -\frac{\alpha_z}{\tau}I_n \end{pmatrix}\begin{pmatrix} y_c - g \\ z \end{pmatrix} \tag{17}$$

This system is linear, and with $\beta_z = \alpha_z/4$ (see [4]) the eigenvalues of the system matrix are given by

$$\mu_{1,\ldots,2n} = -\frac{\alpha_z}{2\tau} \tag{18}$$

Since the eigenvalues are strictly negative, the system (17) is contracting. Further, we note that (11) is hierarchical from (14) to (16). It therefore follows from Proposition 1 that (11) is contracting. This is true for the whole state space. Hence, all solutions of (11) converge exponentially to the same trajectory. Since one solution is given by $\xi = 0$, they must all converge exponentially to this equilibrium point. Thus, (11) is globally exponentially stable. ■

Since $y_a = g$ for $\xi = 0$, Theorem 2 implies that the system (11) converges exponentially to a state where the goal configuration is reached by the actual robot position.

IV. Simulations

The system in Sec. II was sampled at 250 Hz, and the simulations were performed in Cartesian space. For visualization purposes, the dimension of the robot position was set to $n = 2$.

First, a demonstrated trajectory, y_{demo}, was simulated by creating a time series of positions. Thereafter, the corresponding DMP parameters were determined as described in, *e.g.*, [4]. At the start of each simulation, y_0 and y_c were set to the beginning of y_{demo}, and y_a was deliberately initialized with a randomly chosen error with respect to y_0 and y_c.

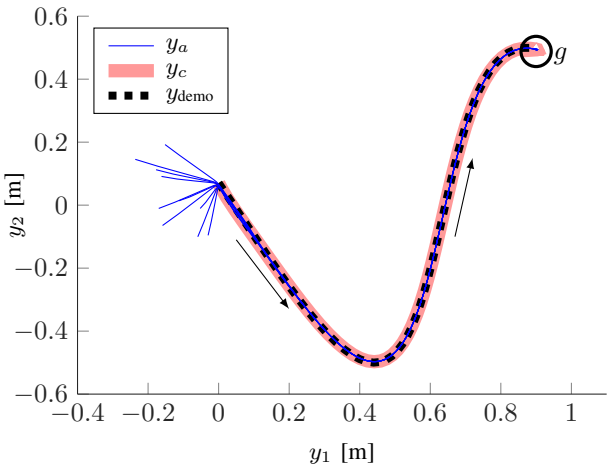

Fig. 3: Positions of simulated trajectories. The movement direction is indicated by the arrows. For an uncluttered view, only 10 of the 100 simulated trajectories are displayed. For each simulation, y_a started to the left in the plot, with some distance to y_c. Then, y_a moved toward y_c. Subsequently, both y_a and y_c converged to the goal position g, which is marked with a circle at the upper right of the plot. Since y_c was initialized to the same point for each simulation, it always followed the same path. Further, it followed the demonstrated path closely, which is expected given a sufficient number of basis functions ($N_b = 50$ were used).

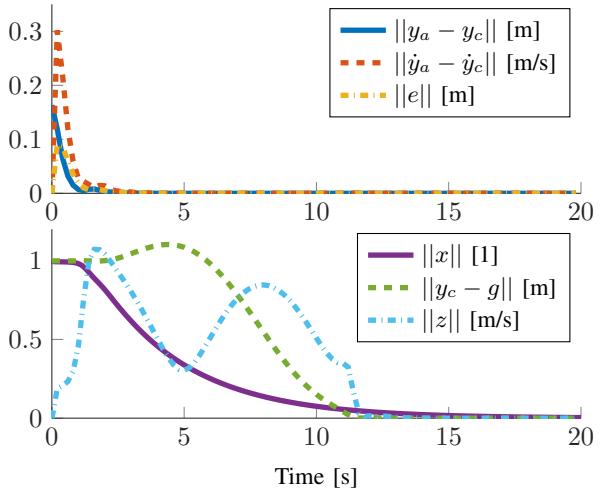

Fig. 4: The magnitudes of the states in (11) plotted over time, for one of the simulations displayed in Fig. 3. The notation $||\cdot||$ represents the 2-norm. It can be seen that y_a converged to y_c, and that e converged to 0. This is expected from Theorem 1. Further, each state converged to 0, which is consistent with Theorem 2.

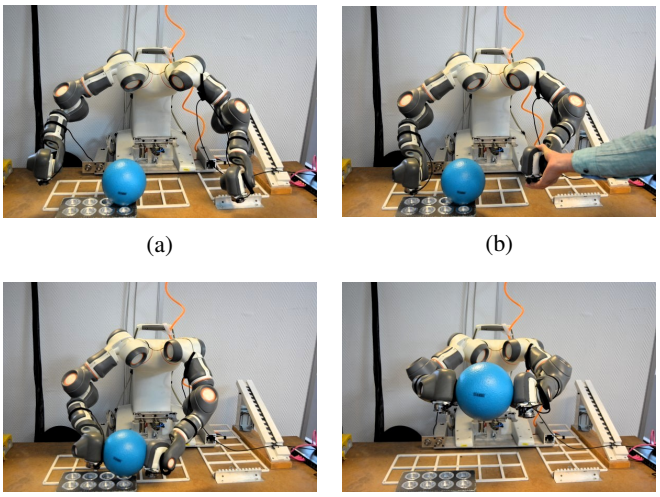

Fig. 5: Setup 3. The robot task was to pick up the blue ball using both arms. The movement started in (a), and a human perturbed the movement in (b). Thereafter, the robot was released and recovered from the perturbation. The arms reached the ball simultaneously in (c). The goal state was then reached in (d).

The purpose of the error was to investigate the convergence of (12). The system was simulated 100 times.

The simulations gave mutually similar results. The results from some of the simulations are visualized in Figs. 3 and 4. For each simulation, the system described by (12) converged to the origin, as predicted by Theorem 1. Similarly, the entire control system described by (11) converged to the origin, as predicted by Theorem 2.

V. Experiments

The algorithm in Sec. II was used to control a prototype of the dual-arm ABB YuMi [14] robot (previously under the name FRIDA), with 7 joints per arm, see Fig. 1. The DMPs were defined in joint space, and hence the total dimension of the configuration space was $n = 14$. The system had the same sampling rate as in the simulations, *i.e.*, 250 Hz.

Four different setups were used to evaluate the stability of the control algorithm. For each setup, 50 trials were made, yielding a total of 200 trials. Prior to each trial, a temporally coupled DMP had been determined from demonstration by means of lead-through programming [20]. In each trial, the temporally coupled DMP was executed while the magnitudes of the states in (11) were logged and saved. Perturbations were introduced by physical contact with a human. The four setups were as follows.

Setup 1. The robot moved its left arm without manipulating any objects. The left arm was subject to two perturbations.

Setup 2. The robot moved both of its arms simultaneously, again without any manipulation. Two perturbations were introduced; first one on the left arm, and subsequently one on the right arm.

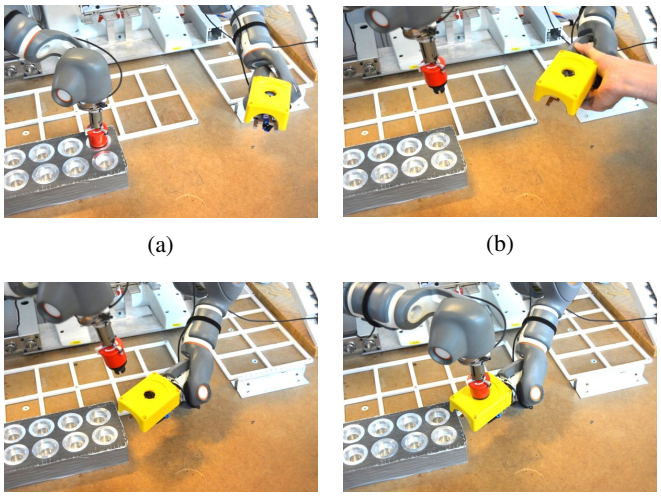

(a) (b) (c) (d)

Fig. 6: Setup 4. The task was to insert the red stop button into the hole in the corresponding yellow case. The initial configuration is shown in (a). In (b), a human perturbed the movement, and in (c) the robot had recovered from the perturbation. The goal configuration was reached in (d).

Setup 3. This setup is visualized in Fig. 5. The robot used both arms to pick up a ball. One perturbation was introduced on the left arm.

Setup 4. This setup is visualized in Fig. 6. The objective of the robot was to mate a stop button, grasped with the right arm, with its corresponding case, grasped with the left arm. The left arm was subject to one perturbation.

A trial of each experimental setup is shown in Part III of the video in [15].

VI. Experimental Results

In each of the 200 trials, the perturbations were first recovered from and thereafter the goal state was reached. Data from one trial of each experimental setup are shown in Figs. 7–10, and the remaining trials gave qualitatively similar results. The figures show the magnitudes of the states in (11) plotted over time. The perturbations are clearly visible in the data. It can be seen that y_a converged to y_c, and that e converged to 0, after each perturbation. This is expected from Theorem 1. The data also show that each state converged to 0, as predicted by Theorem 2.

VII. Discussion

The effect of temporal coupling can be seen in each of Figs. 4 and 7–10. Consider for example Fig. 10, where the robot was grasped by the human at $t \approx 2.5\,\text{s}$. During the perturbation, the evolution of x, y_c and z was slowed down. Such behavior is desired in general, since it helps to retain the coordination between the degrees of freedom of the robot. It resulted from the fact that e had a significant magnitude, which in turn caused τ_a to be significantly larger than τ, see (7). The robot was released at $t \approx 10\,\text{s}$, and the controller described by (8) started to drive y_a to y_c, whereby e was

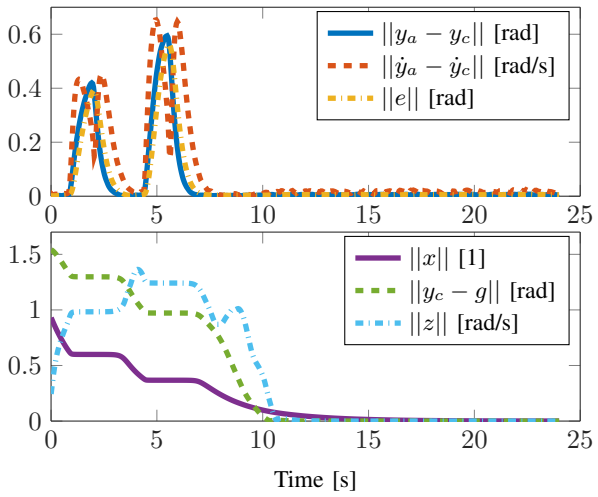

Fig. 7: Data from a trial of Setup 1, where the left arm was perturbed twice during its movement.

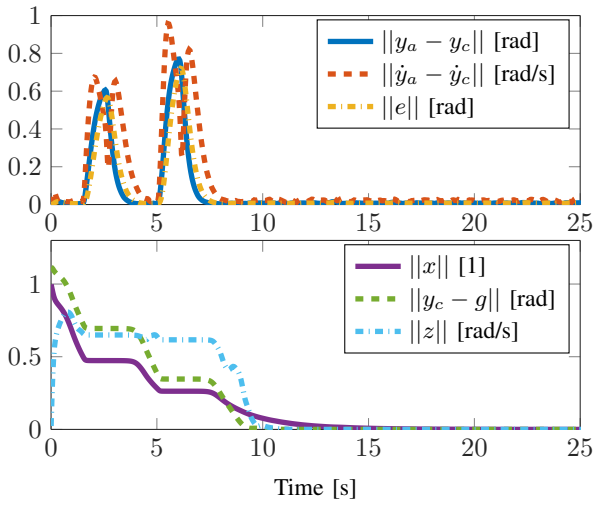

Fig. 8: Data from a trial of Setup 2, where both arms moved simultaneously and were perturbed once each.

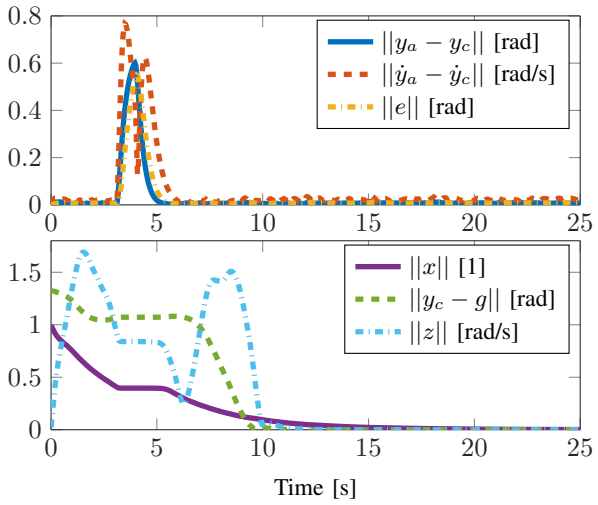

Fig. 9: Data from a trial of Setup 3. The setup is shown in Fig. 5.

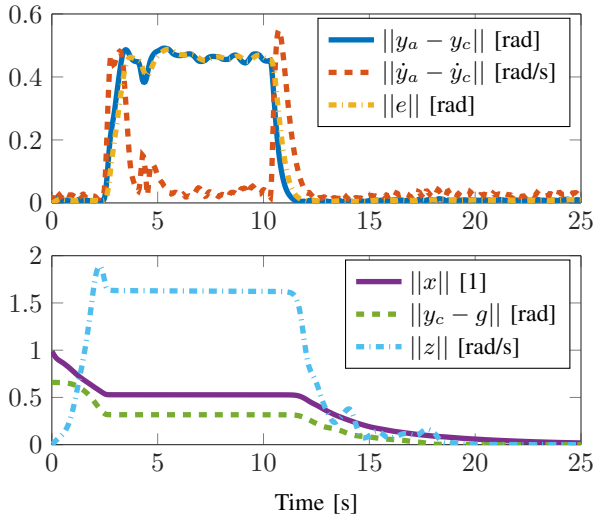

Fig. 10: Data from a trial of Setup 4. The setup is shown in Fig. 6. In this particular trial, the robot was grasped by the human for a significantly longer time than in the trials shown in Figs. 7–9, though this was not the case for all trials of Setup 4.

driven to 0. After e had converged to insignificant magnitude, at approximately 12 s, it can be seen that x, y_c and z evolved considerably faster. The same phenomenon could be seen in each experiment, as well as in the simulations.

In the experiments, the DMPs were defined in joint space. Further, the states in the simulations can for instance be interpreted as joint angles or as positions in Cartesian space. The implementation in joint space allowed the operator to specify the entire configuration on each 7 DOF robot arm, rather than just the tool poses. The DMPs could also have been defined in Cartesian space, see for instance [4], [21]. However, whereas the assumption of a contractible state space in Sec. III is true for the robot joint space and the position in Cartesian space, some care must be taken regarding the orientation in Cartesian space, as discussed in, *e.g.*, [22]. Restrictions on the orientation must be invoked to guarantee that the Cartesian orientation is contained in a contractible space. Finding such restrictions, that are not unnecessarily conservative, remains as future work.

This paper focused on the convergence of temporally coupled DMPs, possibly after perturbations, and not on the perturbations themselves. Even though the perturbations were introduced by physical contact with a human in the experiments presented here, any deviation from the coupled trajectory y_c could be recovered from. For example, the robot could be allowed to take an unforeseen detour to avoid an obstacle. In the experiments, a force sensor was mounted on each wrist of the robot, and the measured forces were scaled and added to the reference accelerations as disturbances, which allowed the human to introduce perturbations in an intuitive way. This arrangement worked well for the sake of evaluating the stability properties of temporally coupled DMPs, and it was straightforward to implement. However, for the purpose of interacting physically with the robot, it would be better to apply passive force control. Such an approach was presented in [8], though temporal coupling was not included. As suggested in [8], it would therefore be interesting to combine temporal coupling with passive force control in the DMP framework in future research.

Some care must be taken when analyzing stability based on contraction theory, because contraction alone does not imply stability. Nevertheless, for autonomous systems, as those considered in this paper, global contraction is equivalent with global exponential stability [19].

Even though Theorem 2 states that the state vector ξ converges to the origin, in practice noise and model errors prevent the state vector from staying arbitrarily close to the origin. In the experiments there was an unmodeled time delay of 12 ms between the controller in (8) and the internal robot controller, which is an example of a model error. In the experiments presented here, the robot end-effectors reached their targets with an accuracy of ± 1 mm. Because the origin could not be reached by ξ with exactly zero error, the movement could for instance be considered finalized once $||\xi|| < \rho$ for some small constant ρ, or upon force-based detection of task completion as in [23]. A related discussion about convergence toward single-point goals can be found in [24]. There, the concept of so-called asymptotic solution plans is also described. Since exponential stability is a stronger requirement than asymptotic stability [16], Theorem 2 implies that temporally coupled DMPs are asymptotic solution plans.

It is important to note that the 'Robot' block in Fig. 2 includes both the robot itself and the internal robot controller. It is possible for the internal control loop to achieve a reference acceleration, $\ddot{y}_r$, with small error, as long as $\ddot{y}_r$ is reasonably smooth and limited in magnitude. Therefore, modeling the robot as a double integrator can be justified as a feedback linearization even though the dynamics of the robot itself (*i.e.*, excluding internal controller) is more complicated than a double integrator.

Stability for the original DMP framework was shown in [12], [13] by utilizing that $f(x)$ converged to 0, which followed from the fact that x decayed exponentially, regardless of any deviation from the intended movement. However, this is true only if temporal coupling is not used, and the convergence of $f(x)$ is less obvious for the DMP version studied in this paper. Due to the adaptive time parameter τ_a in (3), it can not be assumed that x decays exponentially for temporally coupled DMPs. Instead, the stability of temporally coupled DMPs has now been established in the proof of Theorem 2.

The control algorithm in Sec. II includes some parameters that should be chosen, but these have intuitive meanings. To avoid overshoot, the control gains in (8) should be be constrained as described in Sec. II. This yields a negative real double pole for the system (8), located in $-k_v/2$, and a larger magnitude of the double pole corresponds to a faster control system. Similarly, α_z and β_z should be constrained as described in Sec. III and [4]. The control system is intentionally compliant to unforeseen disturbances, such as

contact with a human, and therefore no integral parts are used in the control loop. Introducing integral parts could also yield overshoot in the position domain, which in the context of robotics might result in collision. The constant α_x occurs in previous publications, but it does not affect the functionality as long as it is strictly positive, since it must be compensated for when determining DMP parameters based on desired movements.

Part II of the video in [15] shows the same setups as used in the experiments described in Sec. V, but the original DMP formulation, without temporal coupling, was used instead. Setup 3 and 4 were deliberately designed to require coordination between both arms, in order to highlight the necessity of temporal coupling for DMPs. Without temporal coupling, the coordination was lost in presence of any significant perturbation, and hence these tasks failed in Part II. In fact, the coordination between all DOF of the robot, and not only between the two arms, might be lost. For instance, only the left arm moved in Setup 1, and yet the behavior was not satisfactory in Part II of the video. It can also be noted that the coordination was retained in Part III, despite perturbations, thanks to the temporal coupling.

VIII. Conclusion

In this paper, we addressed the question of whether temporally coupled DMPs are stable. It was shown mathematically that they represent a globally exponentially stable control system, which implies exponential converge to a steady state in which the goal position is reached by the actual robot position. This result was verified in simulations, as well as experimentally on a dual-arm industrial robot.

Appendix

We here consider a passivity property of temporally coupled DMPs. The passivity formalism is described in, *e.g.*, [16], [25].

Theorem 3: Consider the system defined by (11) for DMP operation. The virtual force $f(x)$ can be seen as an external input to the system. The mapping from $f(x)$ to z/τ_a is passive.

Proof: The system is passive if $f(0) = 0$, $\dot{\xi} = 0$ for $\xi = f(x) = 0$, and there exists a C^1 function $V : \mathbb{R}^{5n+1} \rightarrow \mathbb{R}$, called a storage function, for which the following criteria hold [25].

- $V(0) = 0$
- $V(\xi) \geq 0, \ \ \forall \xi \neq 0$
- $\dot{V}(\xi) \leq f(x)^T z/\tau_a, \ \ \forall \xi, f(x)$

Since x is a factor of $f(x)$ and the remaining part of $f(x)$ is bounded, $f(0) = 0$, see Sec. II and [4]. It can further be seen that $\dot{\xi} = 0$ for $\xi = f(x) = 0$.

The states $y_a - y_c$, $\dot{y}_a - \dot{y}_c$, and e have the same dimension, which we denote by n. Let I_n be the identity matrix, and 0_n the zero matrix, each of size n. The upper part of (11) is given by the following linear system.

$$\frac{d}{dt}\begin{pmatrix} y_a - y_c \\ \dot{y}_a - \dot{y}_c \\ e \end{pmatrix} = \begin{pmatrix} 0_n & I_n & 0_n \\ -k_p I_n & -k_v I_n & 0_n \\ \alpha_e I_n & 0_n & -\alpha_e I_n \end{pmatrix}\begin{pmatrix} y_a - y_c \\ \dot{y}_a - \dot{y}_c \\ e \end{pmatrix} \tag{19}$$

Denote by ξ_1 and A_1 the state vector and the system matrix in (19), respectively. Because $k_p = k_v^2/4$ (see Sec. II) the eigenvalues are given by

$$\begin{cases} \lambda_{1,\ldots,2n} = -\frac{k_v}{2} \\ \lambda_{2n+1,\ldots,3n} = -\alpha_e \end{cases} \tag{20}$$

Since $k_v, \alpha_e > 0$, the eigenvalues are strictly negative. Let Q be a symmetric, positive definite matrix of size $3n$. Since A_1 has all eigenvalues strictly in the left half-plane, it follows [17] that there exists a symmetric, positive definite matrix P such that

$$PA_1 + A_1^T P = -Q \tag{21}$$

Now, assume the following storage function V.

$$V(\xi) = \xi_1^T P \xi_1 + \frac{1}{2}x^2 + \frac{1}{2}\alpha_z\beta_z(y_c - g)^T(y_c - g) + \frac{1}{2}z^T z \tag{22}$$

It holds that $V(0) = 0$. Since P is positive definite, any deviation from $\xi_1 = 0$ will give a positive contribution to $V(\xi)$. Similarly, the quadratic terms in (22) guarantee that any deviation from $(x, y_c - g, z) = (0, 0, 0)$ gives a positive contribution to $V(\xi)$. Therefore, $V(\xi) > 0, \forall \xi \neq 0$. Further,

$$\begin{aligned} &\frac{d}{dt}V(\xi) = \xi_1^T P\dot{\xi}_1 + \dot{\xi}_1^T P\xi_1 + x\dot{x} \\ &+ \alpha_z\beta_z(y_c - g)^T\frac{d}{dt}(y_c - g) + \dot{z}^T z \\ &= \xi_1^T(PA_1 + A_1^T P)\xi_1 - \frac{\alpha_x}{\tau_a}x^2 + \alpha_z\beta_z(y_c - g)^T\frac{1}{\tau_a}z \\ &+ \left(\frac{\alpha_z}{\tau_a}(\beta_z(g - y_c) - z) + \frac{1}{\tau_a}f(x)\right)^T z \\ &= -\xi_1^T Q\xi_1 - \frac{\alpha_x}{\tau_a}x^2 - \frac{\alpha_z}{\tau_a}z^T z \\ &+ \frac{1}{\tau_a}f(x)^T z \leq \frac{1}{\tau_a}f(x)^T z, \ \ \forall \xi, f(x) \end{aligned} \tag{23}$$

Hence, a passive mapping from $f(x)$ to z/τ_a can be concluded. ■

Since $f(x)$ represents a virtual force and z/τ_a represents a velocity, the product of these can be interpreted as supplied power to the system. Time integration yields the following

mechanical interpretation of (23).

$$\begin{aligned}\underbrace{V(\xi(t))}_{\text{Stored energy}} &= \underbrace{V(\xi(0))}_{\text{Energy at start}} + \int_0^t \underbrace{f(x)^T z/\tau_a}_{\text{Supplied power}}\,\mathrm{d}t \\ &- \int_0^t \underbrace{\xi_1^T Q \xi_1 + \frac{\alpha_x}{\tau_a}x^2 + \frac{\alpha_z}{\tau_a}z^T z}_{\text{Dissipation power}}\,\mathrm{d}t \\ &\leq \underbrace{V(\xi(0))}_{\text{Energy at start}} + \int_0^t \underbrace{f(x)^T z/\tau_a}_{\text{Supplied power}}\,\mathrm{d}t\end{aligned} \tag{24}$$

Here, integrating the supplied power with respect to time yields total work done by $f(x)$. Hence, the increase in stored energy is not larger than the externally added energy, which indicates passivity.

REFERENCES

[1] S. Schaal, S. Kotosaka, and D. Sternad, "Nonlinear dynamical systems as movement primitives," in *IEEE International Conference on Humanoid Robotics*, September 7–8, Boston, MA, 2000, pp. 1–11.

[2] A. J. Ijspeert, J. Nakanishi, and S. Schaal, "Movement imitation with nonlinear dynamical systems in humanoid robots," in *IEEE International Conference on Robotics and Automation (ICRA)*, vol. 2, May 11–15, Washington, DC, May 11-15 2002, pp. 1398–1403.

[3] A. Ijspeert, J. Nakanishi, and S. Schaal, "Learning control policies for movement imitation and movement recognition," in *Neural Information Processing System (NIPS)*, vol. 15, December 5–10, Stateline, Nevada, December 5-10 2003, pp. 1547–1554.

[4] A. J. Ijspeert, J. Nakanishi, H. Hoffmann, P. Pastor, and S. Schaal, "Dynamical movement primitives: learning attractor models for motor behaviors," *Neural Computation*, vol. 25, no. 2, pp. 328–373, 2013.

[5] F. J. Abu-Dakka, B. Nemec, J. A. Jørgensen, T. R. Savarimuthu, N. Krüger, and A. Ude, "Adaptation of manipulation skills in physical contact with the environment to reference force profiles," *Autonomous Robots*, vol. 39, no. 2, pp. 199–217, 2015.

[6] P. Pastor, M. Kalakrishnan, F. Meier, F. Stulp, J. Buchli, E. Theodorou, and S. Schaal, "From dynamic movement primitives to associative skill memories," *Robotics and Autonomous Systems*, vol. 61, no. 4, pp. 351–361, 2013.

[7] A. Batinica, B. Nemec, A. Ude, M. Raković, and A. Gams, "Compliant movement primitives in a bimanual setting," *arXiv preprint arXiv:1707.04629*, 2017.

[8] M. Deniša, A. Gams, A. Ude, and T. Petrič, "Learning compliant movement primitives through demonstration and statistical generalization," *IEEE/ASME Transactions on Mechatronics*, vol. 21, no. 5, pp. 2581–2594, 2016.

[9] M. Karlsson, A. Robertsson, and R. Johansson, "Autonomous interpretation of demonstrations for modification of dynamical movement primitives," in *IEEE International Conference on Robotics and Automation (ICRA)*, May 29–June 3, Singapore, 2017, pp. 316 – 321.

[10] M. Karlsson, "On motion control and machine learning for robotic assembly," 2017, TFRT–3274–SE, Dept. Automatic Control, Lund University, Lund, Sweden.

[11] M. Karlsson, F. Bagge Carlson, A. Robertsson, and R. Johansson, "Two-degree-of-freedom control for trajectory tracking and perturbation recovery during execution of dynamical movement primitives," in *The 20th IFAC World Congress*, July 9–14, Toulouse, France, 2017, pp. 1959 – 1966.

[12] B. E. Perk and J. J. E. Slotine, "Motion primitives for robotic flight control," *arXiv preprint cs/0609140*, 2006.

[13] P. M. Wensing and J. J. E. Slotine, "Sparse control for dynamic movement primitives," in *The 20th World Congress of the International Federation of Automatic Control (IFAC)*, July 9-14, Toulouse, France, 2017, pp. 10 531–10 538.

[14] ABB Robotics. (2017) ABB YuMi. Accessed 2017-10-24. [Online]. Available: http://new.abb.com/products/robotics/yumi

[15] M. Karlsson. (2017) Convergence of DMPs - experimental evaluation. Automatic Control, Lund University. Accessed 2017-10-24. [Online]. Available: https://www.youtube.com/watch?v=KRfjMXs4LjQ

[16] J. J. E. Slotine and W. Li, *Applied Nonlinear Control*. Prentice-Hall, Englewood Cliffs, NJ, 1991, vol. 199, no. 1.

[17] T. Glad and L. Ljung, *Control Theory*. CRC Press, Miami, FL, 2000.

[18] W. J. Rugh, *Linear System Theory*. Prentice-Hall, Upper Saddle River, NJ, 1996, vol. 2.

[19] W. Lohmiller and J. J. E. Slotine, "On contraction analysis for nonlinear systems," *Automatica*, vol. 34, no. 6, pp. 683–696, 1998.

[20] A. Stolt, F. B. Carlson, M. G. Ardakani, I. Lundberg, A. Robertsson, and R. Johansson, "Sensorless friction-compensated passive lead-through programming for industrial robots," in *IEEE/RSJ International Conference on Intelligent Robots and Systems (IROS)*, September 28–October 2, Hamburg, Germany, 2015, pp. 3530–3537.

[21] A. Ude, B. Nemec, T. Petrić, and J. Morimoto, "Orientation in cartesian space dynamic movement primitives," in *IEEE International Conference on Robotics and Automation (ICRA)*, May 31–June 7, Hong Kong, China, 2014, pp. 2997–3004.

[22] C. G. Mayhew, R. G. Sanfelice, and A. R. Teel, "Quaternion-based hybrid control for robust global attitude tracking," *IEEE Transactions on Automatic Control*, vol. 56, no. 11, pp. 2555–2566, 2011.

[23] M. Karlsson, A. Robertsson, and R. Johansson, "Detection and control of contact force transients in robotic manipulation without a force sensor," in *IEEE International Conference on Robotics and Automation (ICRA)*, May 21–25, Brisbane, Australia, 2018.

[24] S. M. LaValle, *Planning Algorithms*. Cambridge University Press, Cambridge, UK, 2006.

[25] H. Khalil, *Nonlinear Systems*. Prentice-Hall, Englewood Cliffs, NJ, 2002.